IMPACT OF TSUNAMIS ON NEAR SHORE WIND POWER UNITS

A Thesis

by

ASHWIN LOHITHAKSHAN PARAMBATH

Submitted to the Office of Graduate Studies of
Texas A&M University
in partial fulfillment of the requirements for the degree of

MASTER OF SCIENCE

December 2010

Major Subject: Ocean Engineering

Impact of Tsunamis on Near Shore Wind Power Units

IMPACT OF TSUNAMIS ON NEAR SHORE WIND POWER UNITS

A Thesis

by

ASHWIN LOHITHAKSHAN PARAMBATH

Submitted to the Office of Graduate Studies of
Texas A&M University
in partial fulfillment of the requirements for the degree of

MASTER OF SCIENCE

Approved by:

Co-Chairs of Committee,	Juan Horrillo
	Patrick Lynett
Committee Members,	Vijay Panchang
	Prabir Daripa
Head of Department,	John Niedzwecki

December 2010

Major Subject: Ocean Engineering

LIST OF FIGURES

Page

Page

Page

LIST OF TABLES

Page

1. INTRODUCTION AND LITERATURE REVIEW

Wind power units (WPUs) are primarily of three different types, on shore, near shore (Figure 1) and offshore. WPUs lying within three kilometers to the nearest shore line or lying on the water within ten kilometers from the shore are considered a near shore wind turbine. Near-shore wind turbines benefit from the higher coastal winds caused due to differential heating of land and sea. Since the air is denser it has more energy for the same wind speed compared to on-shore winds. The lower cost associated with the maintenance due to easier accessibility makes near-shore wind turbines preferable over offshore wind turbines. Outside the US, especially in Europe, near-shore wind turbines are common, and it is reasonable to assume that wind energy developments in the US will broadly follow the European growth pattern. With the high number of wind farm installations expected to meet the world renewable energy goals over the next decade, there is a continuous increase in the size of the wind power units. This results in an inevitably increasing risk of these vital facilities to be damage by natural events like tsunamis. Tsunami hazard investigation based on NGDC and USGS has shown that parts of the United States such as Puerto Rico and Virgin Islands and U.S Pacific island territories have very high to moderate tsunami threats [1].

This thesis follows the style of *Journal of Earthquake Engineering and Structural Dynamics.*

Figure 1 Near shore WPU susceptible to tsunami hazard, located at Hull, Massachusetts in Boston Harbor

Tsunami is a series of water waves, which is caused by the displacement of a large volume of body of water, usually occurring in an ocean or large lake. Earthquakes, volcanic eruptions, landslides and other mass movements which cause disturbances above and below water have the potential to generate tsunamis. With wave lengths of the order of a couple hundred kilometers and wave heights usually less than a meter, tsunamis are usually long waves at the offshore location. As tsunami waves approach the shoreline where water depth is reduced, their wave lengths reduce to ten to twenty kilometers which implies that the celerity of the waves are reduced. This results in an increase in the height of the waves, which eventually might lead to the collapse or

breaking of the wave. Once broken these waves propagate on to the shore. Among the various ways in which a tsunami can propagate onshore, the common one is that of a rapidly advancing hydraulic bore which is formed by the breaking of the tsunami wave at the offshore reef or at the shoreline. This type of wave front is one of the most destructive forms of onshore propagation of tsunamis (Arnason, Petroff and Yeh, [2]) and this study proposes to use this type of tsunami propagation onto the WPU structure. The bore consists of a turbulent front, which being steep exerts a large force on any objects in its path. In general, tsunami bores might propagate over dry land, in which case they are referred to as a surge or over an existing inundation or flowing water in which case they are called wet bores.

In the past, considerable research has gone into predicting the runup of tsunami waves, as these help to estimate the inundation caused in the coastal areas due to a tsunami. Very few studies have however tried to address the problem of estimating the forces exerted by a tsunami bore on coastal structures. With onshore propagation speeds of the order of nearly 10 m/s and surge heights up to 30 m in extreme cases (Arnason [3]), the force imparted to the coastal structures are considerable. Most of these studies however tried to quantify the forces on vertical walls [4] and other structures which are common among coastal regions. As WPUs have been in existence only recently, there are not any known studies which evaluate the temporal variation of the tsunami force acting on a WPU.

One of the techniques that is used to solve such problems is to experimentally quantify the forces. This, however, poses new challenges, such as the generation of a tsunami bore in a laboratory. Chanson [5] has shown that there exist similarities between a tsunami front and a dam break problem and this fact has been used to tackle the problem of tsunami generation in a laboratory. Dam break problems have been extensively studied in the past and often the tsunami bore is generated by opening experimentally/numerically a gate with water impounded on one side. Chanson [5] had developed a simplified numerical solution to a dam break problem in order to determine its height and velocity. He argued that a dam break resulted in a hydraulic jump which is very similar to a tsunami bore. Then he compared the results that were obtained from the solution of dam break to some of the data sets recorded from tsunami surges on dry coastal plains that had previously occurred. He observed that the solution to the dam break problem was sufficiently capable of predicting the tsunami runup onto the coast. Arnason [3] used the same fact to experimentally create a tsunami bore in a wave tank and allowed it to impinge on a circular/square tubular kept in the wave tank. The same experiment was repeated to determine the forces acting on the cylinder for various bore heights. However, these results are for small scaled models. The result obtained cannot be scaled up to estimate the variation of the forces with time for the actual WPU tower, as determination of a scaling factor would pose a challenging task. Hence in order to simplify the problem, numerical models are needed to be developed to quantify the forces imparted by a tsunami impact. These numerical models however could be validated using the results obtained from the small scaled experiments.

One of the first models to quantify the forces due to a tsunami on a cylindrical structure was developed by Davletshin and Lappo [6]. They studied the tsunami using three different cases. In the first case, the tsunami is treated as a large unbroken wave, in the second, it is treated as a solitary wave, and in the third, the tsunami is treated as a surge, resulting from the breaking of a large wave. They used the shallow water equations to solve the pressure field in the vicinity of a cylinder placed in water. This, however, pose a problem as these shallow water models are incapable of capturing the vertical variation of the velocity/acceleration in case of a tsunami runup and the effects could considerably vary the force acting on objects placed in the flow [7]. The vertical variation of the velocity/acceleration can be captured using a full 3D Navier Stokes Equation (NSE) solver.

The use of solitary waves in the study of tsunami runup onto a coast is quiet common (Synolakis [8], Mo, et al. [9]). The solitary wave, upon reaching shallow depths, breaks and the surge/bore which is formed as a result is allowed to propagate on the coast. But this study proposes to use the dam break method to mimic the last stage of a broken solitary wave to numerically determine forces on a WPU as it is believed that it is able to capture the steep front of an actual tsunami bore/surge. Also the differences in forces due to a bore or surge as shown by Nistor [10] and Yeh [11] are only evident when the dam break method of tsunami generation is used. As shown by the investigators [12] a NSE solver with the free surface tracked using the Volume of Fluids method is capable of capturing the forces due to a dam break. Once the forces have been

determined accounting for these factors; the next task would be to study the impact of these forces on the structural behavior of the WPU.

WPU is a complex structure as it has multiple degrees of freedom (DOF ô).sSome of the DOF ô are rotational DOF ô, sand the deflections violate the small deflection theory. Moreover, a WPU has a gyroscopic moment caused due to the rotation of its blades. These are capable of generating considerable forces in a WPU tower, when coupled with the dynamic response of the WPU tower under the impact of tsunami load. Though some studies have looked into the effect of tsunami loading on different types of structures [13], hitherto no study has looked into the effect of a tsunami loading on a WPU. Hence there is a necessity to determine the dynamic response of the WPU tower to this loading. There is also the necessity of looking into the stresses induced in the structure due to tsunami loading, in order to assess the integrity of the structure under the effect of this loading.

The study also proposes to carry out an experimental validation of the results obtained from dynamic analyses of the structure as a future initiative. The University of California, San Diego (UCSD) has the experimental setup capable of carrying out these validations, which consists of a Large High Performance Outdoor Shake Table (LHPOST), capable of shaking a 65 kW Nordtank Wind Turbine. This setup can also be used to study the effect of the coupling of the dynamics of various components of the WPU with that of the tower.

2. THEORETICAL CONSIDERATIONS

2.1 Hydrodynamic Model

Computational Fluid Dynamics (CFD) is one of the branches of the fluid dynamics that uses numerical methods and algorithms to solve and analyze problems that involve fluid flows. The fundamental basis of almost all CFD problems is the Navier Stokes equation along with the mass conservation equation. These are the governing equations that can describe almost any of the physical properties of a flow. However these equations are very difficult to solve theoretically and require approximations of the same to obtain solutions to problems for practical applications. Various techniques such as finite difference, finite volume, finite element and spectral methods are used to solve these equations.

In this study, a full 3D Navier Stokes equation (NSE) solver is used to model the flow in order to capture the forces exerted by the fluid on the WPU. Two dimensional, hydrostatic models which are usually used to study the progression of tsunami waves take into account only the depth integrated horizontal velocities and the water surface elevations are calculated by the mass conservation equation. These models work well for the determination of tsunami propagation through the ocean. But in case of tsunami generation and runup, the vertical variation of the velocity/acceleration is significant. A Navier-Stokes approach is more suitable for these problems as: 1) it includes the vertical variation of the velocity/acceleration and 2) it helps to better estimate the forces applied by the flow on any structure in the path of the flow. This is because the pressure

obtained from NSE solver is non hydrostatic unlike the depth-integrated long wave models where it is hydrostatic.

2.1.1 Governing Equations and Discretization

The governing equations used to describe the flow of an incompressible, Newtonian fluid in a domain ɱ ȍ, is given by the equation of conservation of mass,

$$\eta \cdot \vec{\nu} = \pi \tag{2.1}$$

and the equation of momentum conservation given by

$$\frac{\partial \vec{\nu}}{\partial t} + \vec{\nu} \cdot \eta \vec{\nu} = -\frac{\rho}{\rho} \eta p + \nu \eta^2 \vec{\nu} + \vec{g} \tag{2.2}$$

where, $\vec{\nu}(\vec{x}, t)$ is the velocity vector of the flow at any point $\vec{x}$ [illegible] at time t, p is the pressure, ρ is the density of the fluid, ν is the kinematic viscosity and $\vec{g}$ is the acceleration due to gravity vector.

In case of the tsunami bore that is studied here, a sharp interface or free surface separates the fluid from the air. The location of this interface is not known before hand and needs to be located. The location of the fluid interface or the free surface is determined using a scalar function $\phi(\vec{x}, t)$ and it satisfies the transport or conservation equation given by

$$\frac{\partial \phi}{\partial t} + \vec{\nu} \cdot \frac{\partial \phi}{\partial \vec{x}} = \vec{\nu} \cdot \eta \phi = \pi \tag{2.3}$$

which states that ϕ propagates with the fluid velocity $\vec{\nu}$. This equation is solved only in the fluid domain.

For solving these equations, the entire domain (both fluid and air) is first discretized into cells which are rectangles (2D) or cubes (3D). Each cell is uniquely identified using a vector ¨ΩΩΩ where ¨Ω ρ and ¨Ω ρ and ¨Ω ρ with ΩΩΩ equal to the number of cells in the and direction respectively. These cells can be of non uniform sizes and this facilitates the use of a higher resolution where the flow parameters vary drastically and lower resolution elsewhere. Each cell has a size given by Ω and Ω in the and direction respectively. The velocity ◊ ¨ΩΩΩ associated with a cell is located at the right, back and the top face of the cell. The parameters such as pressure ¨ΩΩΩ , volume of fluid fraction ¨Ο¨ΩΩΩ, are located at the center of the cell (described in 2.1.4).

For any flow in a domain, the parameters such as ◊ and ¨Οare known at time π. The governing equations can then be solved by discretizing them spatially and temporally in order to obtain the flow parameters in the domain at any required time.

2.1.2 Temporal Discretization

The continuity equation (2.1) and the momentum equation (2.2) are discretized in time by using an explicit forward Euler method, which reads

$$\eta \supset \rangle \pi \tag{2.4}$$

and

$$\frac{\diamond \wedge \circ \diamond}{\neg Y} \quad \diamond \supset \eta \quad \diamond \quad \frac{\rho}{} \quad \eta \eth \wedge \circ \quad \eta \cdot \neg \wedge \quad \acute{\varepsilon} \tag{2.5}$$

The subscript ά indicates the time level, i.e ά is the old time level and ά طى ρ for the new time level and T is the time stepping. The continuity equation is discretized at the new time level ά طى ρ in order to preserve a divergence free velocity field. In the momentum equation, all terms are discretized at the old time level except the pressure term. The solution to equation 2.4 and 2.5 is solved by a two fractional steps projection method (Chorin [14] and Harlow and Welch [15]). The two fractional steps are given by

ۿطيۿ ◊ ؏ / ″Y طي شي ◊ Ↄɳ ◊ ؏ طى ʉɳ· ″Ⅰ؏ طى ἐ (2.6)

and

◊ ؏ ᴧ ० طي ۿ / ″Y طي شي ρ / ″؏ ɳƉ؏ ᴧ ० (2.7)

where equation (2.6) is an explicit expression for the intermediate velocity field ۿ referred to as the predictor step and equation (2.7) is an implicit expression for the new velocity field ◊ ؏ ᴧ ० termed as the projection step. In equation (2.6), all terms are explicit and known from the previous time level or initial condition, so the intermediate velocity field ۿ can be easily determined. If the pressure gradient term is discretized at the old time level, then both the continuity equation and the momentum equation could predict a velocity field at the new time level (◊ ؏ ᴧ ०), which may not necessarily be equal. So it is attempted to apply a correction to the intermediate velocity ۿ field by discretizing the pressure at the new time level, so that the new velocity field is divergent free (Gerrits [16]).

This results in an equation obtained by combining equation (2.7) and the continuity equation (2.4), which can be solved to obtain the pressure at the new time level given by

$$\nabla \cdot \left(\frac{\rho}{\Delta t}\nabla p^{n+1}\right) = \frac{\nabla \cdot \vec{u}^{*}}{\Delta t} \tag{2.8}$$

which is known as the Pressure Poisson Equation (PPE). The finite difference of this equation would result in a system of linear equation which can be solved iteratively using methods such as successive over relaxation (SOR), generalized minimal residual(GMRES) and incomplete Cholesky conjugate gradient. From here the velocity field at the new time level ($\vec{u}^{n+1}$) can be determined by substituting this value in projection step, which becomes

$$\vec{u}^{n+1} = \vec{u}^{*} - \frac{\Delta t}{\rho}\nabla p^{n+1} \tag{2.9}$$

2.1.3 Spatial Discretization

2.1.3.1 Continuity Equation

To ensure global mass conservation, i.e., the total amount of fluid in the entire computational domain, and local conservation, i.e., the amount of fluid in the computational cell, the change in the surface level must be consistent with the mass fluxes. For sake of simplicity consider a two dimensional (2D) computational cell (Ω_{ij}) in the domain. The control volume at cell center, x_i, y_j is bounded by $x_{i-1/2}$, $x_{i+1/2}$ and $y_{j-1/2}$, $y_{j+1/2}$ as shown in Figure 2. For spatial discretization, first the continuity equation (2.1) is discretized and results in

$$u_{i,j} A_{Ri,j} \delta y_j + v_{i,j} A_{Ti,j} \delta x_i - u_{i-1,j} A_{Ri-1,j} \delta y_j$$
$$- v_{i,j-1} A_{Ti,j-1} \delta x_i = 0 \qquad (2.10)$$

where $u_{i,j}$ is the horizontal velocity at the right face of the cell, $u_{i-1,j}$ is the horizontal velocity at the left face of the cell, $v_{i,j}$ is the vertical velocity at the top face of the cell and $v_{i,j-1}$ is the vertical velocity at the bottom face of the cell. $A_{Ri,j}$ is the area fraction open to the flow at the right face of the cell, $A_{Ri-1,j}$ is the area open to the flow at the left face of the cell, $A_{Ti,j}$ is the area open to the flow at the top face of the cell and $A_{Ti,j-1}$ is the area open to the flow at the bottom face of the cell.

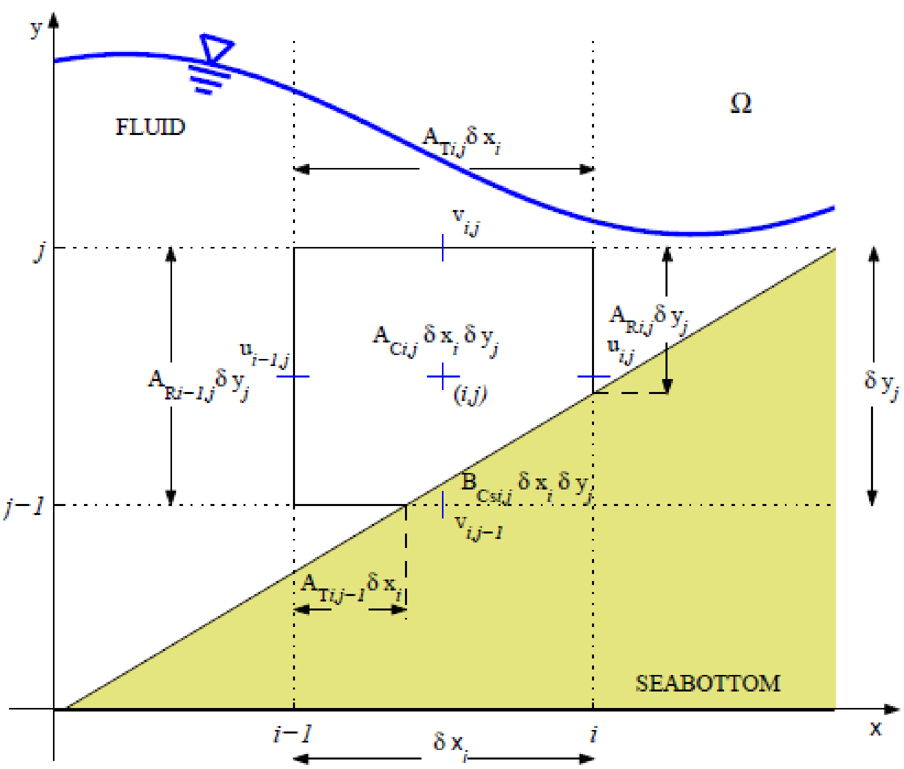

Figure 2 Two dimensional grid cell for the discretization of the continuity equation

Area fraction is the quantity that decides how much of the cell is open to a flow. This is used, because partly blocked cells, such as the ones near an obstruction or at the bottom, if treated as a completely blocked cell, would result in a discrete step, which is not desirable especially when modeling complex geometries. Hence an area fraction is determined for every cell, which is the fraction of the area, at a particular face open to the flow or in other words, it is the fractional aperture of the cell that is open to the flow. This technique of using area fraction is also known as Fractional Area Volume Obstacle Representation (FAVOR), Nichols et al [12]; Sicillan and Hirt [17]; Gentry et al [18].

2.1.3.2 2D Momentum Equation Discretization

The momentum equation (2.2) is discretized in the ὼand ώdirection as

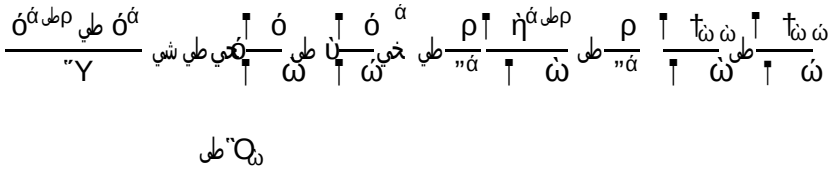

(2.11)

and

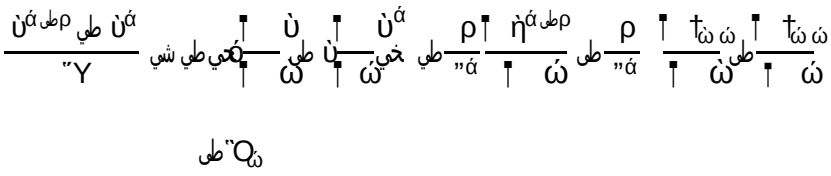

(2.12)

In these equations, the advection term is in the non conservative form. These terms are again discretized using a) backward/forward/central difference method (first or second order approximation), b) third order accurate method. Among these the first

order approximation is used in this study a

approximations of the velocity.

2.1.4 Free Surface Tracking, Volume of Fluid (VOF)

In the computational domain, it is assumed that the fluid has a constant density given by "ي and the density of air is zero. The scalar quantity, Volume of Fluid for a cell is defined as ‟Oسي$\frac{ق}{ق_{ه}}$, where " is the density of cell. This implies that a value of ‟Oسي π implies that the cell is a void cell, ‟Oسي ρindicates a completely filled cell and πحى‟Oحى ρ implies that cell is a free surface cell. The volume of fluid is transported through the fluid using the transport equation as shown below

$$\frac{‟Ω‰‟O¶}{‟Ω ò}_{ط}\frac{‰‟O ق}{¶ ù}_{ط}\frac{‰‟O ù}{¶ ú}_{سي} π \qquad (2.13)$$

where ‰ accounts cell aperture open to the flow. The temporal discretization of the above equation is given by

$$‟O_{ج^{٨٠}}سي‟O_{ج^{٨٠}}ط\frac{¨Y}{ö_{كلي}}\frac{ρ}{¶ ù_{ج}}\ ö_{ز كلي}ó_{ج^{٨٠}ق}\ طي خثث ö_{ز كلي}ó_{ج^{٨٠}ق}\ و كلي ó_{ج^{٩٠ه}ق}\ خ ث ة$$
$$ط\frac{ρ}{¶ ú_{ج}}\ ö_{ا كلي}ù_{ج^{٨٠}ق}\ ح طي ö_{ا كلي}\ و كلي ù_{ج^{٩٠ه}ق}\ خ ج \qquad (2.14)$$

where the bracketed ق‟Óis the amount of volume fraction entering a particular cell at that face. The spatial discretization of the ‟Ofunction is done using the donor acceptor method as described by Hirt and Nicholes [19], which is a geometric solution for the volume of fluid fraction entering or leaving a cell, accounting for the effect of free surface. A detailed explanation of the donor acceptor method is not shown here.

2.1.5 Boundary Conditions

The boundary conditions that are used in this study are the wall boundary condition, the outflow boundary condition and the velocity boundary condition. The boundary conditions are set by defining the value of the flow parameters in the ghost cells. Ghost cells are an additional row/column of cells which are located outside the boundary of the real cells as shown in Figure 3. The use of these ghost cells is to set the boundary conditions for the flow. Unlike the other cells in the domain, the values of the flow parameters are set in the ghost cells and not calculated using the governing equations. Once the flow parameter values are set, the flow parameters in the rest of the domain is calculated using the governing equations and the set parameters of the ghost cells, enter into the calculation.

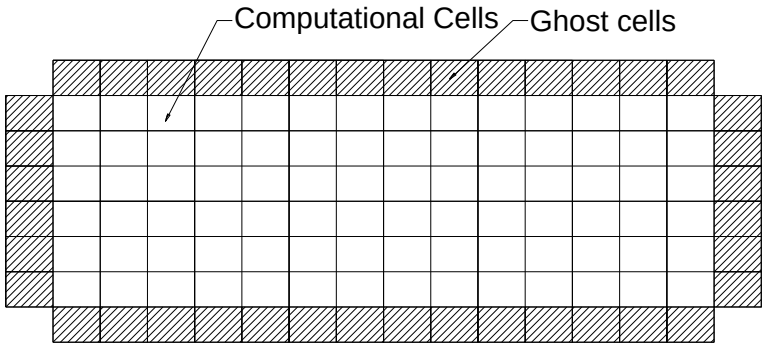

Figure 3 Computational domain with ghost cells and real cells

The various boundary conditions are set as shown below.

2.1.5.1 Wall Boundary Condition

The wall boundary condition is when any fluid that reaches that cell is not allowed to pass through that cell. The method for accomplishing this is shown using an example of a wall boundary at a minimum ὡboundary. The values for the first real cell is set as

ό₀ ᾰᾰ سي πẞπ

ὴ₀ ᾰᾰ سي ὴ. ᾰᾰ

῞Q ᾰᾰ سي ῞Q ᾰᾰ (2.15)

"₀ ᾰᾰ سي ". ᾰᾰ

2.1.5.2 Outflow Boundary Condition

The outflow boundary condition, also known as the radiation boundary condition is the one that permits all the fluid that reaches that point to exit the domain without causing significant effects in the upstream location. Usually the flow is only required to be modeled in a specific region of the entire fluid domain and these boundary help to cut off the computational mesh, beyond the region where flow characteristics that are not required to be calculated. The outflow boundary condition is set by using the Sommerfeld radiation boundary condition, which is a simple mathematical continuation having the form of outgoing waves,

$$\frac{\partial \phi}{\partial n} + \frac{1}{c}\frac{\partial \phi}{\partial t} = \pi \qquad (2.16)$$

where ϕ is any quantity and n is directed out of the boundary and c is the local phase speed of the wave or flow.

2.1.5.3 Velocity Boundary Condition

The velocity boundary condition is set by changing the velocity in the ghost cell to the value defined by the user. It is possible to vary the velocity defined in the ghost cell with respect to time. The fluid height is also set here. The VOF values of the ghost cells are set depending on whether the cell is a filled cell, void cell or a surface cell.

2.1.6 Stability Criterion

The stability of the numerical approximation is assured by automatically changing the size of the time step based on the Courant–Friedrichs–Lewy (CFL) condition and the maximum pressure iterations condition. The CFL criterion for any cell in the computational mesh is given by

$$\frac{u\,\delta t}{\delta x} \le 1 \qquad (2.17)$$

Above expression controls the time steeping according to the velocity field and cell size. The time step is adjusted automatically by searching the maximum velocity in the fluid domain and compared against the allowable velocity in that particular cell. If the velocity exceeds a pre-established value the time stepping is reduced by 5%.

2.1.7 FLOW-3D

The above mentioned equations are implemented in FLOW-3D, which is a commercial CFD tool that is capable of solving a wide variety of physical flows. Some of the salient features of FLOW-3D are:

- It uses FAVOR method
- Computational grid and geometry are independent
- Can handle internal, external and free surface flows
- Can handle one, two and three dimensional flows
- It can solve transient flows which are inviscid, viscous, laminar and turbulent
- Can track fluid interfaces using the VOF method
- Advection terms with approximation up to the third order can be solved
- Can track sharp fluid interfaces
- Has implicit and explicit modeling options
- Has the GMRES and SOR implementation for the pressure solver
- Can handle many different types of fluid boundaries such as rigid wall, continuative, periodic, outflow, hydrostatic pressure, etc.
- Provisions for changing some of flow properties at runtime using the restart option
- A robust data visualization tool, to visualize the various flow properties such as, but not restricted to pressure, free surface, velocities, cell fluid fractions and forces on objects placed in the flow

All these features make it a robust tool for carrying out our study and have been used to solve the hydrodynamic problem.

2.2 Structural Stress Analysis Model

The ANSYS Structural package is used to carry out finite element structural analysis of the WPU tower structure. The tower which is basically a thin-walled cylinder made up of three sections, of varying cross sections, is discretized using 4-noded shell elements. These elements have six degrees of freedom (along three lateral and three rotational directions) at each of their nodes and they are capable of accounting for variable shell thickness at each node. However in this study, the shell thickness is considered constant. The spatial discretization (rectangular) of the model is obtained using the automatic meshing capability of the structural stress analysis package. The tsunami loads are applied as nodal loads at each shell elements along its degree of freedom direction. The thin-walled cylinder is fixed at the bottom using a full fixed boundary condition, i.e. all the displacements and rotations are restrained at the bottom. The force-stiffness relationship is used to determine the forces induced in the shell element due to the nodal loads. The forces are then used to determine the principal stresses induced in the shell elements. The equivalent stresses or Von Mises stresses induced in the structure are then determined.

2.3 Structural Dynamics Model

For the purpose of carrying out a dynamic structural analysis, the whole WPU tower is

idealized as a dynamic system having 30 discrete masses with each mass having 3 degrees of freedom, two lateral displacements along the ώhŭώand one rotational displacements along the ΄Yώdirection. The coordinate system for carrying out the dynamic analysis is oriented such that the ώ›axis is along the length of the WPU. The nacelle (refer Appendix A) and the rotor are idealized as masses at a point at the hub height of the WPU. The tower is fully fixed to the ground by restraining all displacements and rotations.

The dynamic analysis of the WPU is carried out using the modal superposition method. The mass matrix used in the analysis is determined using the consistent mass matrix method. The damping associated with each modal frequency has been experimentally obtained [20]. The procedure for obtaining the response of the structure is as shown below.

According to D'Alembert's principle, any system that has a mass and is subjected to acceleration would develop an inertial force proportional to its acceleration and opposing it. If a given N degree of freedom structural system has stiffness and damping associated with each of its degrees of freedom, the force equilibrium equation for this system can be written in the following form as a set of N second order differential equations

$$M\ddot{x} + C\dot{x} + Kx = F \qquad (2.18)$$

where ╜ is the mass matrix, ╒ is damping matrix, ╚ is stiffness matrix of the system, ╕ ò is the time history of the force applied on the system, ó ò is the time history of the response of the system. Further ╕ ò can be expressed in the form

$$╕\ ò\ سي\ ﻫﺠ\ █▌\ ò\ ج \qquad (2.19)$$

which means that time dependent loading can be represented by a sum of ɑὐɛ space vectors █ which are not a function of time, and ɑὐɛ time functions ▌ ò ج where ὐ cannot be greater than the number of displacements N. This is another way of saying that each mass is acted upon by a maximum of only one force along each degree of freedom. Equation (2.18) is solved by method of separation of variables. A solution to the equation can be expressed in the form

$$◊\ ò\ سي\ ز\ ╨\ ◄ \qquad (2.20)$$

where ز is an ñ N by L ò matrix (not a function of time) which vectors represents the position of the Nth mass in the Lth mode of vibration and ╨ ò is a vector containing L functions of time, which represent the variation of the Lth mode with respect to time. ز is also known as the mode shape of the structure. The ز is chosen such that it satisfies the stiffness and mass orthogonality condition

$$ز\ \text{Ɛ}ز\ ῆ\ سي\ ἓ$$
$$ز\ ῆ\ ἓ\ ز\ سيص˥ \qquad (2.21)$$

where I is the diagonal identity matrix and ω is a diagonal matrix, which may or may not be the free vibration frequencies of the system. This equation (2.21) is then substituted in equations (2.18) and (2.19) to obtain

$$\ddot{q}_n + 2\zeta_n\omega_n\dot{q}_n + \omega_n^2 q_n = \sum_{j=1}^{m} \Gamma_{nj} P_j(t) \qquad (2.22)$$

where Γ_{nj} and is known as the modal participation factors for time function $P_j(t)$ The modal participation factor for the n^{th} mode is given by ϕ_{jn} This factor is an indicator of how much a particular mode participates in the response of the structure.

The damping matrix is usually not a diagonal matrix, but it is assumed to be so that the equations are uncoupled and this results in a diagonal matrix C given by

$$C_{jj} = 2\zeta_j\omega_j \qquad (2.23)$$

where ζ_j is defined as the ratio of the damping in mode j to the critical damping of the mode. Hence the typical uncoupled modal equation, for a linear structural system can be represented as

$$\ddot{q}_j + 2\zeta_j\omega_j\dot{q}_j + \omega_j^2 q_j = \sum_{j=1}^{m} \phi_{jn} P_j(t) \qquad (2.24)$$

Now if we have an arbitrary modal time history loading, which is piecewise linear and given by $P(t)$ as shown in Figure 4, the equation (2.24) can be expressed as

$$\ddot{q}_j + 2\zeta_j\omega_j\dot{q}_j + \omega_j^2 q_j = P(t) \qquad (2.25)$$

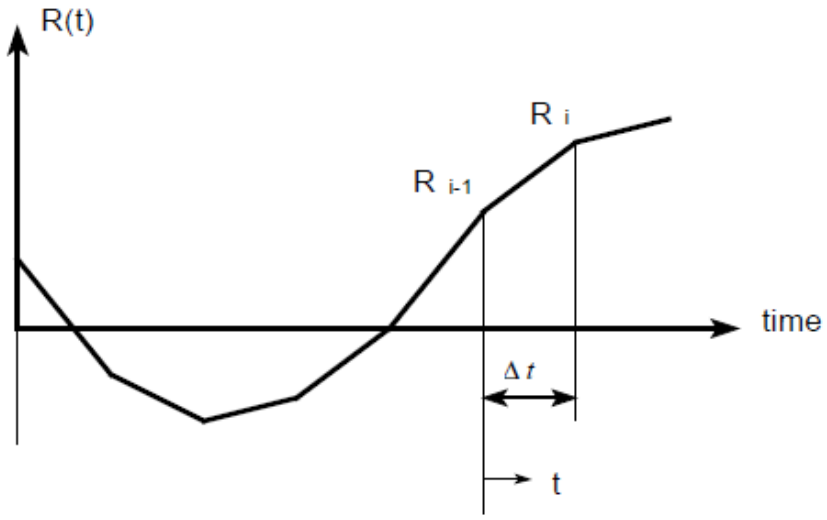

Figure 4 Typical modal load function

This equation (2.25) can now be solved by using finite difference method to obtain the values of responses ώ ò ẗώ ò and ώ ò. A detailed description of the numerical methods to solve this is given by Clough, Penzien [21]. In this study the structural analysis software SACS is used to carry out this computation.

3. VALIDATION

3.1 Hydrodynamic Model versus Experimental Setup

Before FLOW-3D, henceforth referred to as the hydrodynamic model, can be used to capture the forces exerted by a tsunami bore on a WPU, it has to be verified against the dam break problem. This is done by validating the hydrodynamic model using the data obtained from an experimental study carried out by Arnason et al. [2]. The experimental setup consists of a tank that is 16.62 m long, 0.61 m wide and 0.45 m deep. The tank has a pneumatically activated gate at 5.9 m away from the upstream end of the tank. The gate can be lifted very quickly (~2 m/s) to simulate a dam break like condition in the tank. The experimental study uses specific impoundment depths of water in the upstream side of the gate (Refer Table 1) and at downstream (20 mm constantly) locations. A cylindrical column having a diameter of 140mm is placed at a distance of 5.2 m from the gate. A sketch of the experimental setup is shown in Figure 5 for clarity. The gate is lifted and the water is allowed to impinge on the cylinder. The time history of the force exerted by the water on the cylinder is then determined. This data are available for validating (Figure 6) the numerical models (Arnason [2]).

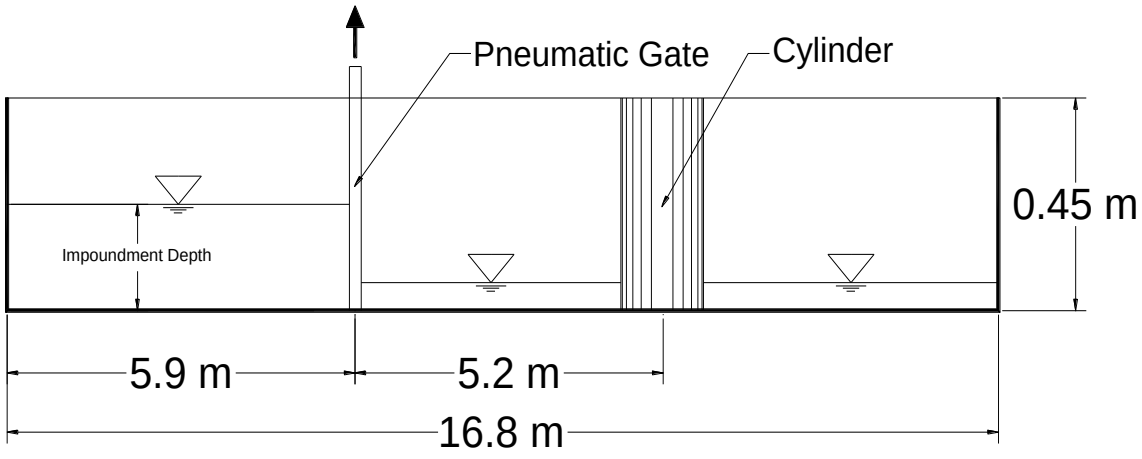

Figure 5 Experimental setup used to validate hydrodynamic model (Arnason, Petroff and Yeh [2])

The same set of physical experiments is reproduced using the hydrodynamic model with domain size and resolution indicated in Table 1. The hydrodynamic model has a provision for defining an initial water depth in the upstream and downstream location at time t = 0 sec. The water gradient is then allowed to flow under the effect of gravity in a bore like form towards the cylinder. The hydrodynamic model is capable of capturing the free surface elevation (sharp discontinuity), velocity vectors, pressure and the forces acting on the cylinder. The time history of the force acting on the cylinder for various impoundment depths are shown in Figure 7 (Page 27).

Table 1 Computational domain specifications for different impoundment depths

S.No	Impoundment Depth(mm)	Domain Size	Number of Cells	Cell Size		
		LxBxH (m x m x m)	NX x NY x NZ	DX (m)	DY (m)	DZ (m)
1	100	16.6 x 0.6 x 0.45	332 x 48 x 9	0.09 - 0.01	0.015-0.01	0.05
2	125	16.6 x 0.6 x 0.45	332 x 48 x 9	0.09 - 0.01	0.015-0.01	0.05
3	150	16.6 x 0.6 x 0.45	332 x 48 x 9	0.09 - 0.01	0.015-0.01	0.05
4	200	16.6 x 0.6 x 0.45	332 x 48 x 9	0.09 - 0.01	0.015-0.01	0.05
5	275	16.6 x 0.6 x 0.45	332 x 48 x 9	0.09 - 0.01	0.015-0.01	0.05
6	300	16.6 x 0.6 x 0.45	332 x 48 x 9	0.09 - 0.01	0.015-0.01	0.05

3.2 Comparison of Results

Figure 6 and Figure 7 show a comparison of the forces on the cylinder obtained experimentally and using the hydrodynamic model. They show a very good correlation. It is observed that the forces obtained from the hydrodynamic model follow the same trend as the experimentally. This agreement indicates that the hydrodynamic model is capable of capturing most of the characteristics of the flow portrayed in the experimental study. It is also observed that the forces imparted on the cylinder increases as the impoundment depth increases, which has also been shown in the studies by Nistor et al [10] and Yeh [11]. It is determined that the hydrodynamic model over estimates the load on the cylinder by 8 to 23 percentages (Refer Table 2). It is also determined that the percentage error in the estimation of the force decreases as the impoundment depth increases. This is promising as it is usually a challenging task to match the forces exerted

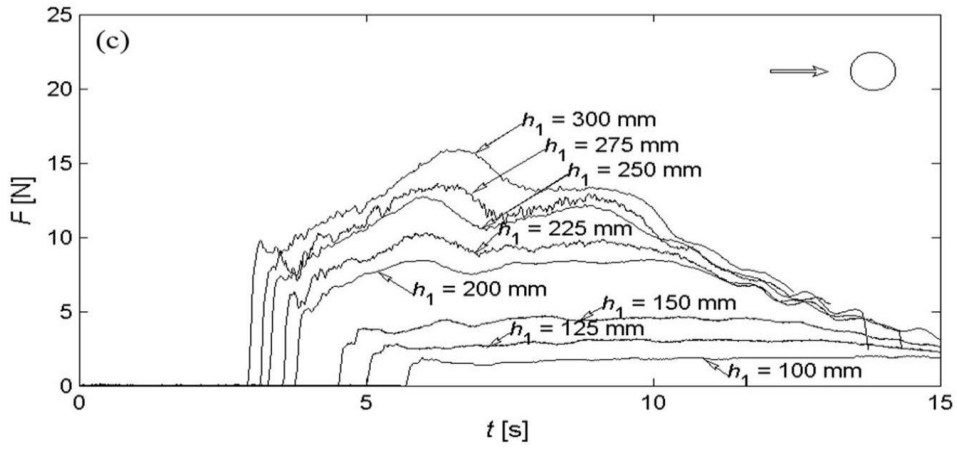

Figure 6 Forces acting on cylinder from Arnason et al [3] experiment

on objects placed in a fluid to experimental data, unlike surface elevations which are relatively much easier to match. However, in this validation case, the sampling rate of the forces is considerably low and decided based on the CFL criteria for the computational domain. A better correlation to the experimental results can be achieved by altering the time step size by limiting the maximum time step in the hydrodynamic model.

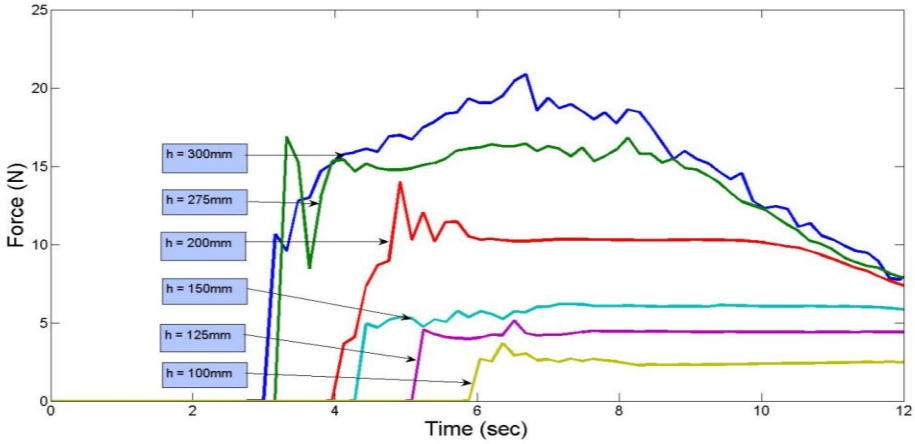

Figure 7 Forces acting on cylinder calculated by FLOW3D

Table 2 Percentage difference in the estimation of forces (Experimental v/s Hydrodynamic model)

S.No	Impoundment Depth	Maximum Force		Difference (%)
		Experimentally(N)	Numerically(N)	
1	100	3.0	3.68	+22.67
2	125	3.8	4.56	+20.00
3	150	4.9	5.29	+7.95
4	200	9.8	10.50	+7.14
5	275	14.3	15.40	+7.69
6	300	18.0	19.35	+7.50

3.3 Conclusions

As observed, the hydrodynamic model only slightly overestimates the load acting on a cylinder placed in the fluid. The overestimation of forces means that the safety of the structure is not compromised. The overall economy of the design obviously seems to be sacrificed, but since the probability of occurrence of the tsunami load is low it would result in smaller safety factors on this load for design purposes and thereby neutralize the effect of overestimation of forces. A detailed investigation of safety factor considering hydrodynamic model uncertainty and tsunami risk is beyond the scope of this study. Since the validation results look acceptable for the purpose of determining the forces on the cylinder, the hydrodynamic model is used in the study to determine the forces acting on the actual WPU tower.

4. QUANTIFICATION OF FORCES ON WPU

Three surge cases and three bore cases are modeled using the hydrodynamic code. A bore/surge is usually formed after the tsunami wave is broken near the shore. A tsunami being a long wave, the wave celerity is given by $\sqrt{g d}$ where g is the acceleration due to gravity and d is the depth of flow. The computational domain that is modeled begins after the wave has broken and progresses through it the form of a bore/surge. Modeling of tsunami bore/surge using the hydrodynamic model involves the following steps:

4.1 Establishing a Computational Domain

The right handed coordinate system (Figure 8) for the hydrodynamic computational mesh is oriented such that the X- direction is directed along the fluid flow into the domain. The Y-direction is oriented perpendicular to the direction of the flow. The Z-direction is in the upward direction. For the purpose of determining the hydrodynamic forces on the WPU, it is idealized as a cylinder having a diameter equal to the base of the WPU tower. The cell sizes are not uniform throughout the mesh. It has finer resolution near the face of the cylinder in the X and Y direction (Figure 9). This is because the front of the tsunami bore is very steep just before impacting on the cylinder and smaller cells will be capable of better capturing the pressures around the cylinder and hence force field on the cylinder. Again reducing the cell size does not necessarily guarantee a better result from a practical perspective as the increase in accuracy after a specific threshold cell size is not worth the computa

carrying out the simulation. The specifications of the computational mesh for the various surge/bore cases are given in Table 3. The flooding/upstream impoundment depths used in the bore impact cases are shown in Table 4. The flooding depth has an impact on the force exerted by the bore on the WPU tower. This is due to the enhancement of the momentum flux behind the front of the bore due to the non uniform velocity profiles within the bore (Svendsen and Madsen [22]).

Table 3 Specification of computational domain for determining forces on WPU

Case	**Height**	**Domain Size**			**Number of Cells**	**Cell Size Range(m)**		
	(m)	**L (m)**	**B (m)**	**H (m)**	**NX x NY x NZ**	**DX**	**DY**	**DZ**
Bore/ Surge	2	50	5.0	6.0	266 x 50 x 60 = 0.798 million	0.40 - 0.10	0.15 - 0.10	0.10 - 0.10
	5	50.0	5.0	11.0	266 x 50 x 110 = 1.463 million	0.40 - 0.10	0.15 - 0.10	0.10 - 0.10
	10	50.0	5.0	20.0	266 x 50 x 220 = 2.926 million	0.40 - 0.10	0.15 - 0.10	0.10 - 0.10

Table 4 Impoundment depth and flooding depth

S.No	Impoundment Depth (m)	Flooding Depth (m)
1	2	0.5
2	5	0.5
3	10	1.0

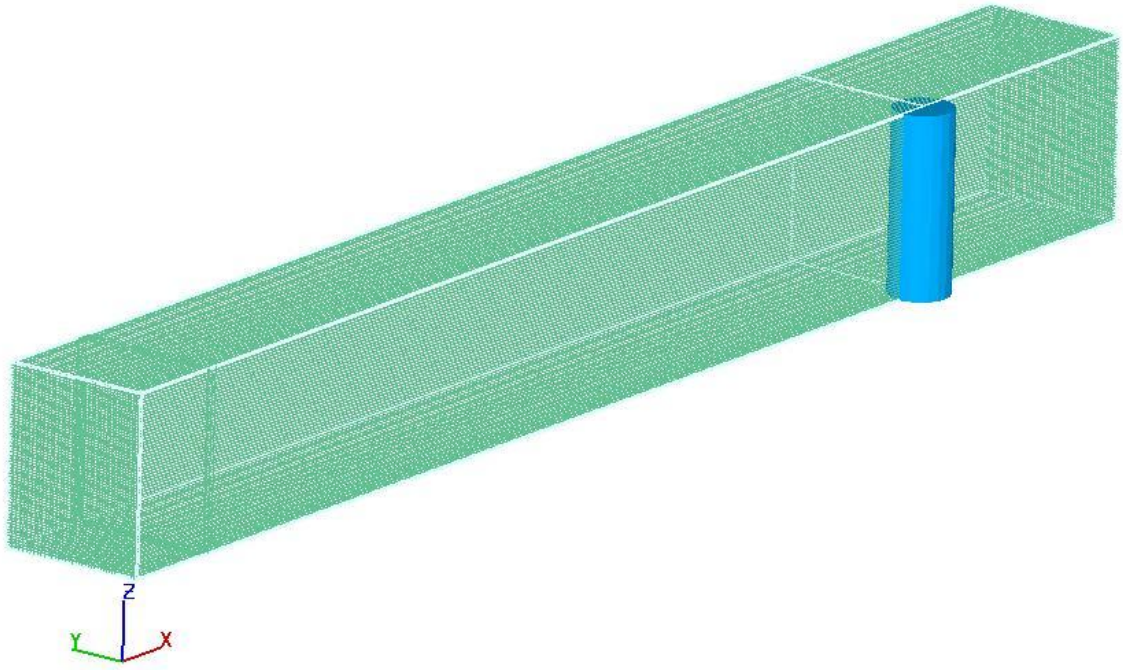

Figure 8 Computational domain and orientation of the coordinate system

It is assumed that the flow is almost symmetrical about the XZ plane, which means only one half of the flow needs to be modeled in order to capture the forces excreted on the cylinder. This helps to drastically reduce the total run time and the computational resources required to simulate the model without inducing significant error in the analysis. Assuming a symmetrical flow means that the effect of vortex induced vibrations (VIV) of the WPU tower is not considered in the dynamic analysis of the structure. However the effect of the VIV would be significantly lesser when the bore/surge impinges the tower as the VIV would not be fully formed immediately after the front impinges the cylinder.

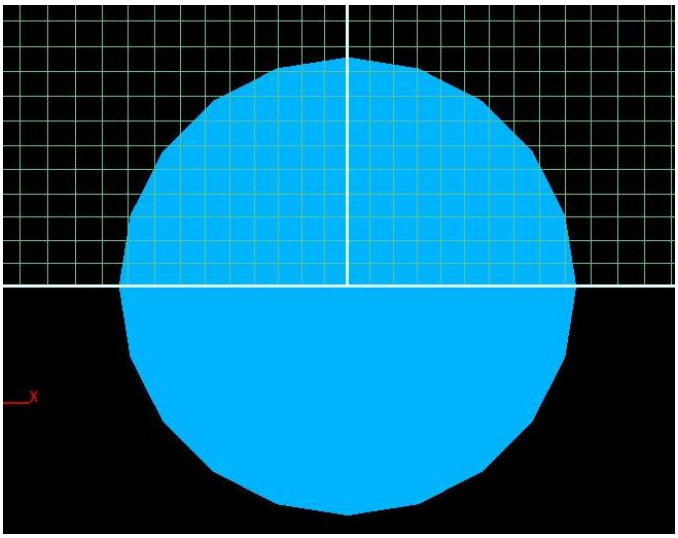

Figure 9 Mesh resolutions near the cylinder

4.2 Physics Constrains

The fluid is assumed to be inviscid and incompressible. The governing equations are solved in an Eulerian frame of reference where gravity is the driving force. The effect of surface tension has been neglected at the interface between fluid and void. The bottom friction is based on slip condition. Density is assumed to be constant throughout the fluid domain. The effect of air entrainment at the surface of the flow has not been considered in the analysis. Compressibility of the air at the fluid air interface will increase the force acting on the cylinder as compressed air is capable of exerting additional pressure on the face of the cylinder as opposed to a void.

The effect of turbulence is not accounted for in the hydrodynamic model. Previous studies (Svendsen and Madsen [22]) have shown that the turbulence would start at a

location behind the front of a bore increases in thickness behind the front. This turbulence would spread towards the bottom as the bore propagates. An investigation into the variation in forces because of this is beyond the scope of this study.

4.3 Boundary Conditions

The bore/surge is input into the computational domain using a velocity equal to the wave celerity and a fluid height equal to the bore/surge height. The inflow boundary at the upstream end of the fluid domain is modeled using the velocity boundary condition. This sets the fluid height in the ghost cell to the value specified by the user and the velocity drives the flow into the domain as described by the VOF transport equations. Since our primary interested is in the forces exerted on the cylinder, which is influenced only by the flow field in the vicinity of the cylinder, it is not necessary to model the flow in the downstream locations at a reasonable distance away from the cylinder. Hence the downstream end of the fluid domain has outflow boundary condition, which permits the flow reaching that boundary to exit the domain. This is accomplished as shown in section 2.1.5.2. The upper boundary of the fluid domain is also modeled as an outflow boundary condition as this helps any stray sprays/volume of water, generated by the splashing of the fluid on the cylinder to leave the domain. These hardly influence the forces on the cylinder, even if they are reflected from the top, but make the visual interpretation of the flow patterns difficult. The other boundary conditions in the flow are rigid wall boundary conditions, which do to permit any fluid to enter or exit the domain.

4.4 Numerical Schemes

The time step size for the simulation is determined by the model using the stability and convergence criterion as described in section 2.1.6. The generalized minimal residual (GMRES) method based implicit scheme pressure solver is used to solve the momentum equation. Momentum advection is approximated using the first order terms.

4.5 Simulation

Model simulation is carried out using both processors on a dual core computer. The simulation time for the various surge/bore cases are shown in Table 5. The simulations time is the real time taken by a particular case. The elapsed time is how the wall time the computer takes to simulate the case. This includes the time taken to read input files and generate output files. The CPU time indicates the time taken by the processors in the actual computation and excludes the time taken for input/output tasks. The CPU time is nearly two times the actual wall time in the cases shown below, since the hydrodynamic model is run in parallel on two processors. The hydrodynamic model is actually scalable up to 8 processors as long as the computer has a shared memory architecture. A shared memory architecture is when every processor on the computer, doesnôt ha dedicated memory but shares a single main memory. An interesting observation here is that the hydrodynamic model took 335600 sec (~ 3 days and 22 hours) to simulate 27.5 seconds of the 10 m bore case, which has a total of 2.9 million cells in its mesh! This is undoubtedly a major disadvantage of using the full 3D Navier Stokes equation solver in non parallelized systems. The simulation of flow is carried out with a time step that does

not exceed 0.001 seconds. This is not to meet the stability condition but to record forces with sufficient resolution to carry out a dynamic analysis.

Table 5 Computation times for various surge/bore cases

Case	Height (m)	Simulation Time (sec)	Elapsed Time (sec)	CPU Time (sec)
Bore	2	30	5715	9750
	5	30	16770	30460
	10	27.5	335600	644505
Surge	2	30	5066	8513
	5	30	8630	15210
	10	27.5	330600	611500

4.6 Discussion of Results

Plots showing the temporal variation of one of the cases (5m surge) is shown in Appendix C. The time history of the force acting on the cylinder for the various cases is shown in Figure 10, Figure 11 and Figure 12. It can be seen that the bore cases exhibit a steeper rise in force at the time of impact. This is due to the steeper face of the bore front when it impacts the cylinder compared to a surge. This agrees well with the observations by Yeh [11] in his study of bore and surge runup of tsunamis on coastal structures. The force computed by the hydrodynamic model seems to exhibit a lot of numerical noise. This is due to a pressure spike, which is a due to various consequences as shown by

Fekken [23]. One reason is the presence of an obstruction, cutting a cell face at an angle, which is unavoidable in case of a cylindrical object. Another cause could the air entrainment, which occurs when a free surface impacts an object. There might be a bubble bursting inside the fluid and this shows up as a spike and this is not unphysical. As shown by Fekken [23], filtering these can be quite cumbersome, and this makes it difficult to be included in this study. But since the pressures predicted by the hydrodynamic model is pretty close to the actual results as shown in the validation and also since these spikes do not cause any instability in the model, only a simple filtering of the force signal, above a critical frequency of 50 Hz has been performed.

.

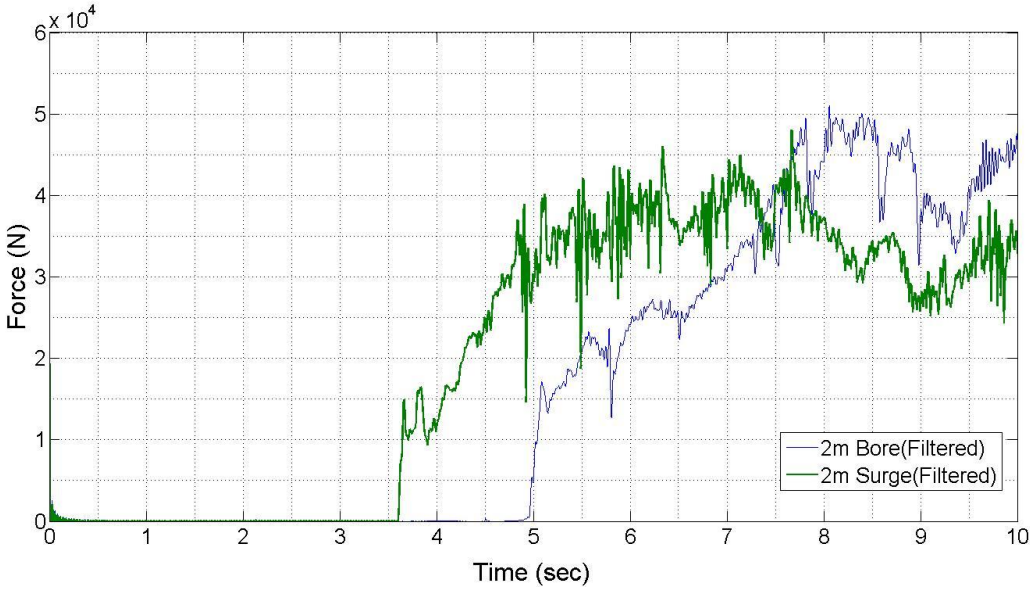

Figure 10 Forces on cylinder due to 2 m bore/surge

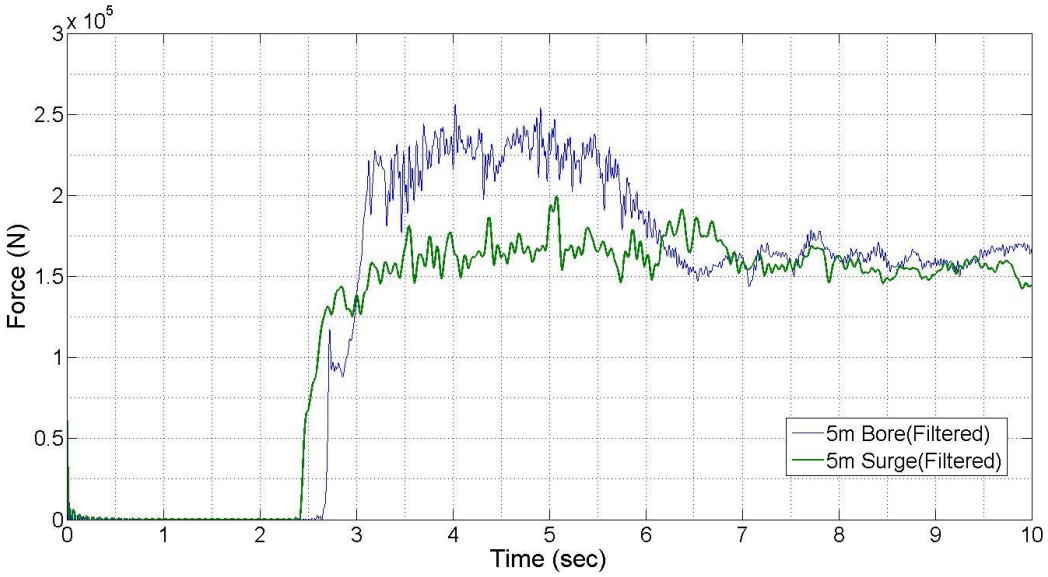

Figure 11 Forces on cylinder due to 5 m surge/bore

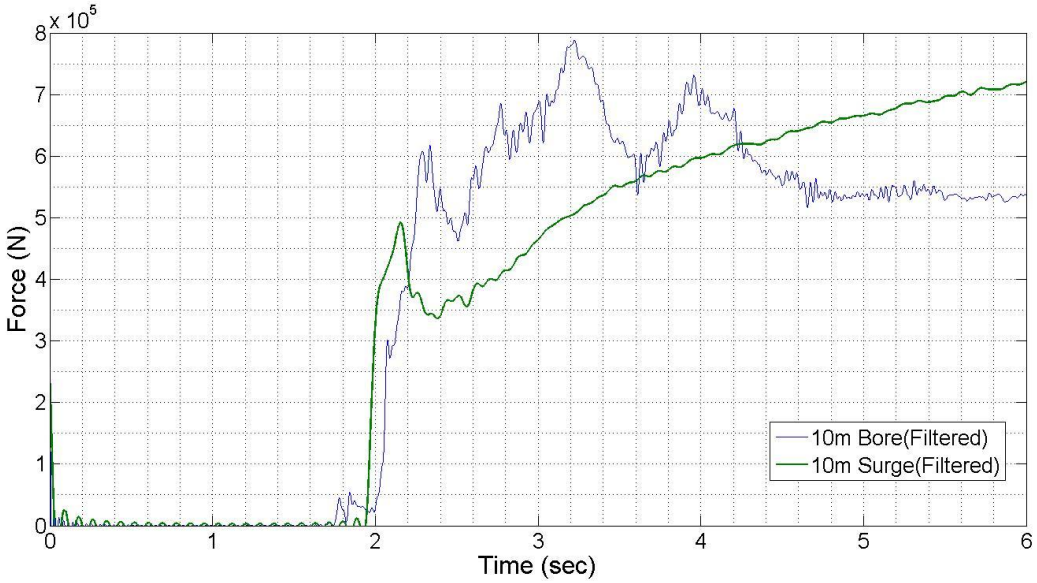

Figure 12 Forces on cylinder due to 10 m surge/bore

5. STRUCTURAL RESPONSE AND INTEGRITY

Once the forces exerted by the tsunami on WPU are quantified, the impact of the forces on the WPUôs structural integrity is investigated. Firstly the stresses induced by the load on the tower structure are determined by using a simplified static analysis of the WPU. For this, a FEM structural analysis of the cylinder is carried out using ANSYS to quantify the stresses induced in the structure due to the hydrodynamic loads in addition to the already existent loads on the structure. Secondly the dynamic behavior of the structure is investigated by carrying out a simplified dynamic structural analysis of the WPU tower.

5.1 Description of WPU

The WPU tower used for this study is the 65kW Nordtank wind turbine manufactured in Denmark. These turbines were produced in large number in the early California for utility scale power generation [24] and by 1985 accounted for nearly 40% of all wind turbines in California [24]. This turbine is much smaller than the multi mega watt turbines of modern day, but they have more or less the same structural configuration as the large ones. The primary reason this type of turbine is used in this study is because University of California, San Diego has one mounted on top of a shake table. This experimental setup can be used to determine the structural response of the WPU under the effect of a base excitation. It is shown later that this setup can be used to experimentally determine the dynamic response of the WPU under tsunami loading conditions. The important characteristics of the WPU are shown in the table on page 41.

5.2 Static Structural Analysis

5.2.1 Numerical Modeling

The preliminary static structural analysis is carried out to determine the stresses induced in the tower section at the point of impact of the tsunami load. The pressure field from the hydrodynamic model is imported into the structural model to perform a structural stress analysis.

The turbine tower is modeled as a cylinder having a diameter of 2.02 m, 5.3 mm wall thickness and a height 15 m. The weight of structure and the components above 15 m are replaced by its weight. This is because it was observed after preliminary analyses that the increase in stresses die down exponentially away from the point of application of the load and extra stiffness imparted by significantly influence the stress distribution in the cylinder, near the point of impact of the load.

The meshing of the turbine tower in ANSYS is done using 4 noded rectangular plate elements, which means every node is attached to exactly four elements. ANSYS's smart sizing option is used to automatically generate the mesh. The mesh has a resolution of 3 mm in the X and Y direction and 0.12 m in the Z direction. The steel is assumed to be elastic. 1.0×10^{11} Pa and Young's Modulus ratio of 0.29 and a density of 7850 kg/m^3.

The pressure distribution at the nodes of the hydrodynamic model is used to compute the value of pressure at the nodes of the structural model. Nodes of the hydrodynamic model refer to the center of each cell in the hydrodynamic model and FLOW-3D reports the value of the fluid properties at that point. Since it is difficult to determine the exact value of the pressure at a structural node, the value of the pressure at the six neighboring nodes are averaged to get the pressure at the node. Once the pressure at a structural node is obtained, it is assumed that it is constant over one-fourth of the area of all the four elements that are shared by that node. A typical sketch is shown for clarity (Refer Figure 13). In the figure, N1 denotes the structural node, P(1-6) are the FLOW-3D node where pressure values are available and Area of N1, is the area used to calculate the force to be applied at node N1. The force is applied at the node in the XY plane in a direction perpendicular to the face of the cylinder.

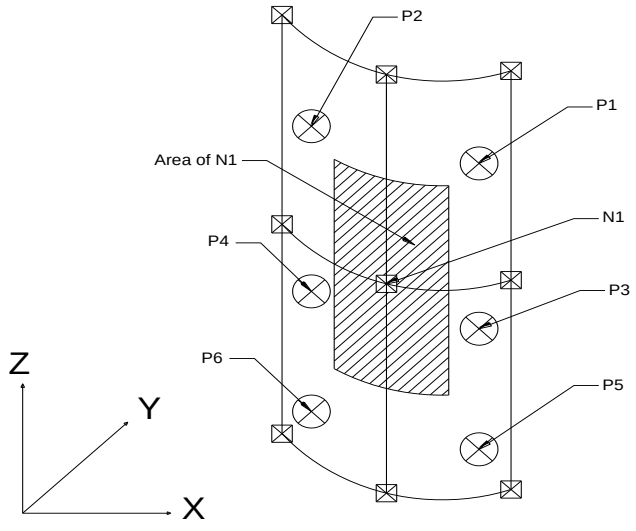

Figure 13 Determination of forces at the structural node

The analyses are carried out (for the WPU described in Table 6) and the results are shown on pages 43 to 48.

Table 6 Properties of 65kW Nordtank Turbine. Source [20]

Property	**Value**
Rated power	65 kW
Rated wind speed	34 km/h (21 MPH)
Rotor diameter	16.0 m (628 inches)
Tower height	21.9 m (864 inches)
Lower section length	7.96 m (313 inches)
Lower section diameter	2.02 m (78 inches)
Middle section length	7.94 m (312 inches)
Middle section diameter	1.58 m (62 inches)
Top section length	6.05 m (238 inches)
Top section diameter	1.06 m (41 inches)
Tower wall thickness	5.3 mm (0.20 inches)
Rotor hub height	22.6 m (888 inches)
Tower mass	6400 kg (14 kips)
Nacelle mass	2400 kg (5 kips)
Rotor mass (with hub)	1900 kg (4 kips)

5.2.2 Discussion of Results

It is observed that the Von Mises Stress is higher in the case of a bore impact, as is

expected based on the studies by Yeh [11] and Nistor [10] (see Figure 10, Figure 11 and Figure 12). Since the yield stress of the steel is 248 MPa (36 ksi), the tower structure is adequately safe for the case of a 2 m bore (Figure 14) and surge (Figure 15) case as the maximum Von Mises stress is found to be 151 MPa and 28 MPa in the two cases respectively. The maximum utilization factors in the structure are given by 0.91 and 0.17 respectively. The utilization factor is defined as the ratio of the calculated stress to the allowable design stress. The allowable design stress is taken as the minimum of two third of yield stress. For the case of the 5 m bore (Figure 16) and surge (Figure 17) cases, the maximum Von Mises stresses are found to be 257 MPa and 259 MPa. The maximum stresses are found at locations near the base of the WPU tower, where it connects to the fully fixed support. Even though the structure has stresses above the permissible limits, with utilization factors equal to a maximum of 1.55 and 1.57 respectively, the structure can still be assumed to be safe. This is because the tower is modeled as only as a cylindrical shell. Additional structural elements such as internal stiffeners, connection detailing and other appurtenances have not been considered for the structural analysis. Significant additional stiffness will be imparted to the structure if these are also considered in the analysis and hence making it safe. Also the fully fixed condition is an idealized concept which is very rarely achieved in real life. There would be considerable flexibility at supports and this would help to reduce the stresses induced in the tower structure. Such tower structures usually have flanges which are connected to the base of the tower through bolted connections and this would also help to reduce the stresses in the structure. On the other hand, the probability of drifted object impact on a tsunami

event is of high concern and requires meticulous and complex study, meaning a substantial impact at this level of stresses would jeopardize the structure integrity. The stresses in case of the 10 m bore (Figure 18) and surge (Figure 19) cases are 1610 MPa and 1560 MPa respectively. This clearly indicates a structural failure of the tower structure as the maximum utilization factors are 9.75 and 9.45 respectively.

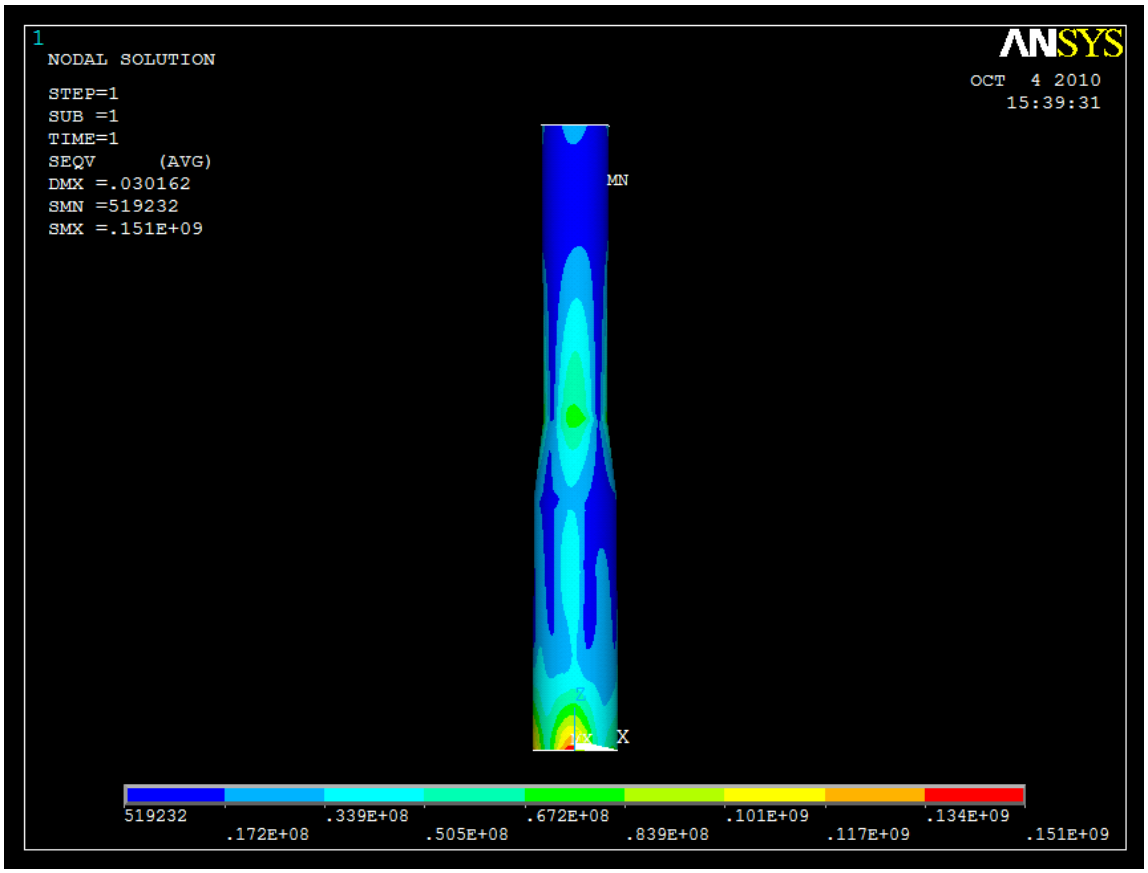

Figure 14 Stress distribution along WPU due to 2 m bore (unit: Pa)

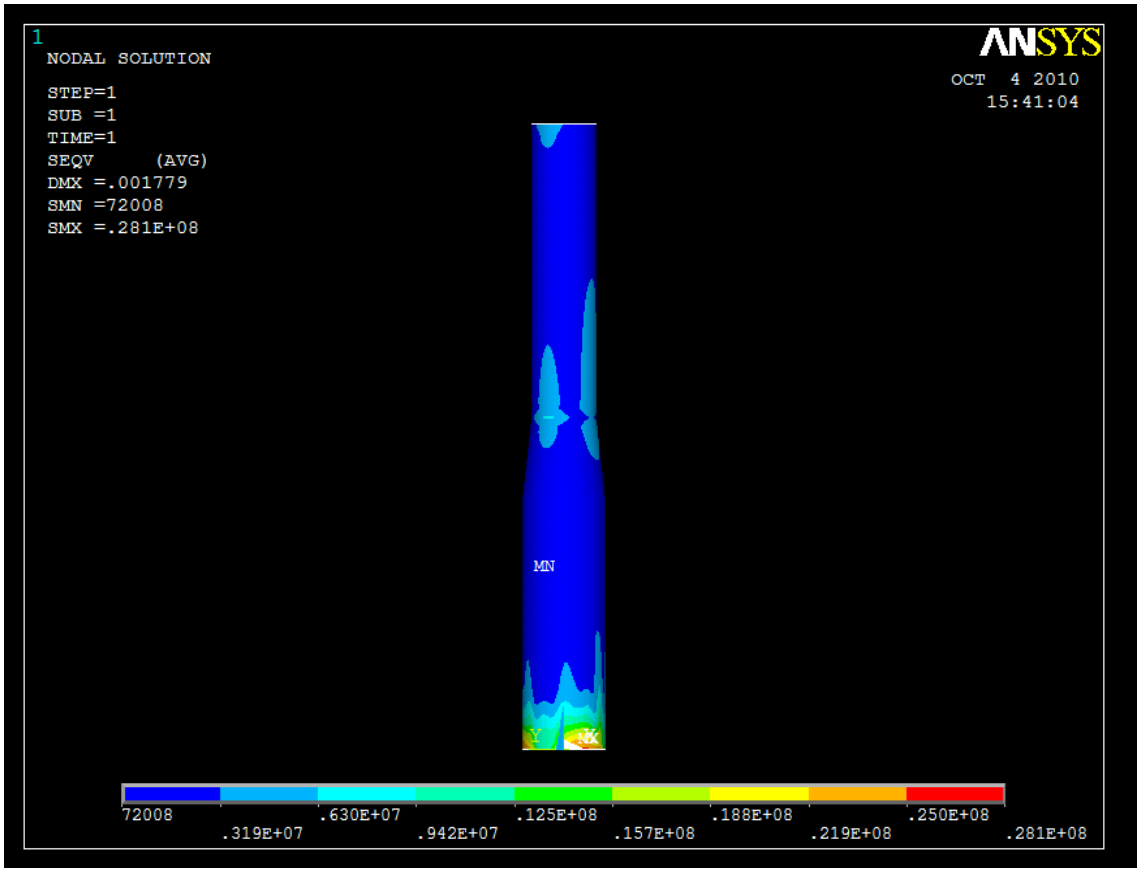

Figure 15 Stress distribution along WPU due 2 m surge (unit: Pa)

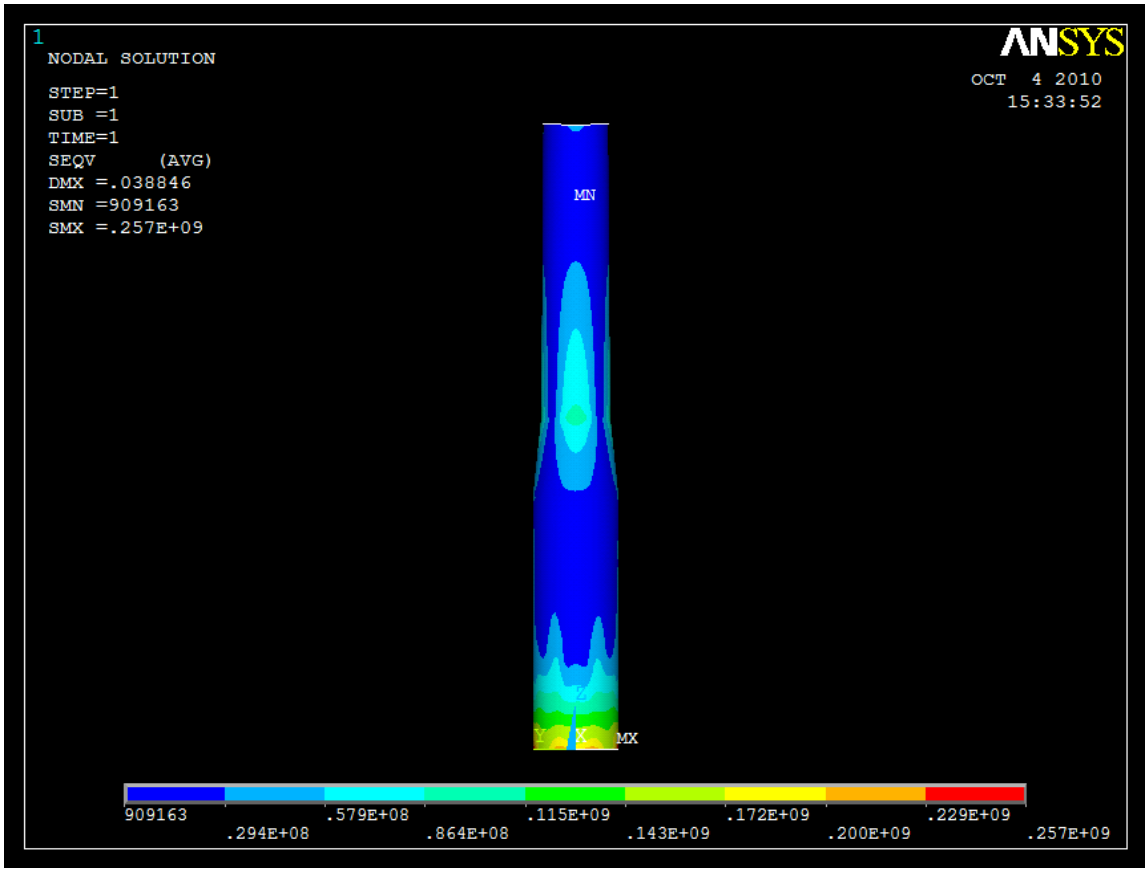

Figure 16 Stress distribution along WPU due to 5m bore (unit: Pa)

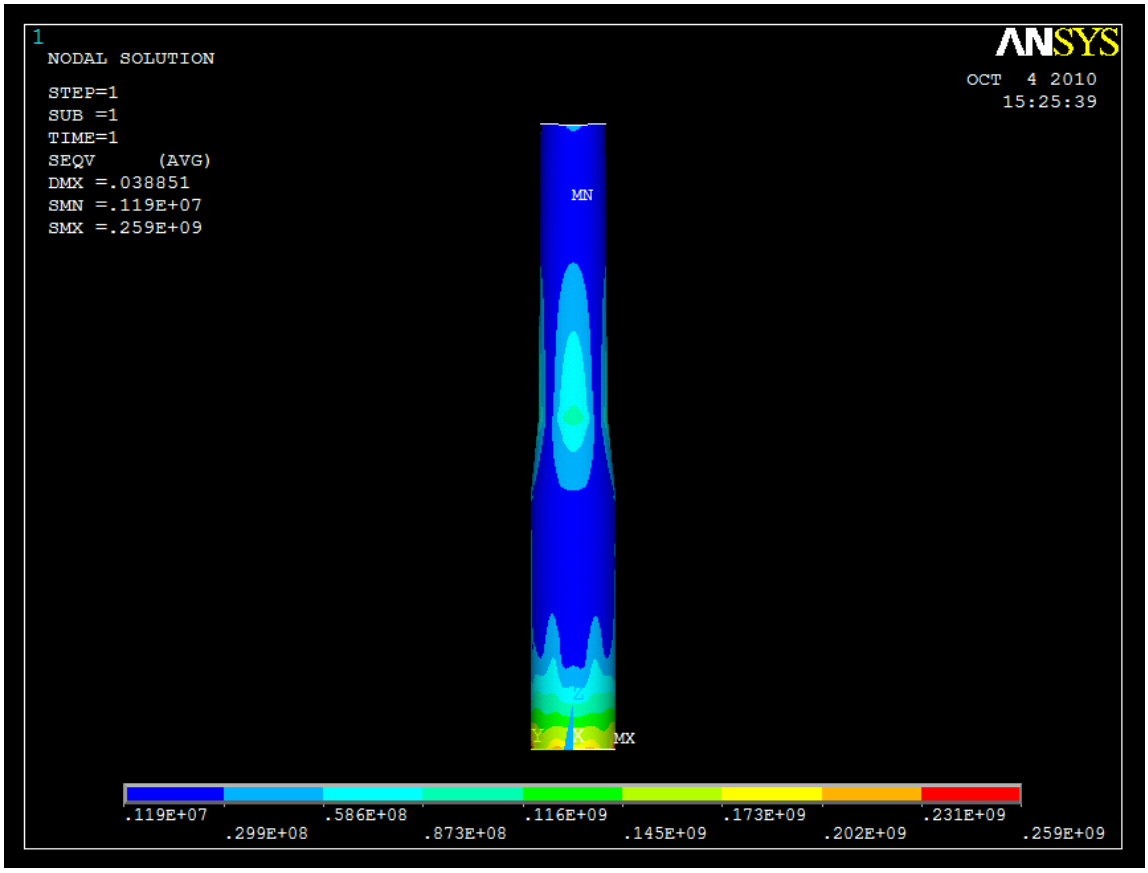

Figure 17 Stress distribution along WPU due to 5 m surge (unit: Pa)

Figure 18 Stress distribution along WPU due to 10 m bore (unit: Pa)